Adsorption of Pb(II) from Aqueous Solutions onto Humic Acid Modified by Urea-Formaldehyde: Effect of pH, Ionic Strength, Contact Time, and Initial Concentration

Meidita Kemala Sari[1], Rahmat Basuki[2,3], and Bambang Rusdiarso[4*]

[1]*Master Programs, Department of Chemistry, Faculty Mathematics and Natural Science, Universitas Gadjah Mada, Sekip Utara, PO BOX BLS 21, Yogyakarta 55281, Indonesia*

[2]*Doctoral Programs, Department of Chemistry, Faculty Mathematics and Natural Science, Universitas Gadjah Mada, Sekip Utara, PO BOX BLS 21, Yogyakarta 55281, Indonesia*

[3]*Department of Chemistry, Faculty of Military Mathematics and Natural Sciences, Universitas Pertahanan RI, Bogor 16810, Indonesia*

[4]*Department of Chemistry, Faculty Mathematics, and Natural Science, Universitas Gadjah Mada, Sekip Utara, PO BOX BLS 21, Yogyakarta 55281, Indonesia*

Corresponding author:

tel: +62-8156860897
email: brusdi_mipa@ugm.ac.id

Received: March 9, 2021
Accepted: July 22, 2021

DOI: 10.22146/ijc.64600

Abstract: *Humic acid (HA) and urea-formaldehyde (UF) have been frequently reported as heavy metal adsorbents. However, the literature has never written HA modification by UF to improve the adsorbent's performance. In this study, a new adsorbent of humic acid-urea formaldehyde (HA-UF) was synthesized. The reaction of the conducted the formation of HA-UF –COOH group of HA with the –NH_2 group of UF was evidenced by decreasing total acidity from 549.26 cmol/kg (in HA) to 349.30 cmol/kg (in HA-UF). The success of HA-UF formation was characterized by attenuated total reflection-infrared (ATR-IR), energy dispersive X-Ray (EDX), and X-ray diffraction (XRD). The high stability of HA-UF was shown by 96.8% remaining in solid form at pH 12.4. Adsorption behavior of Pb(II) onto HA-UF was influenced by the ionic strength and pH, which were mainly driven by the ion exchange mechanism (E_{DR} = 9.75 kJ/mol). The higher ionic strength will affect decreasing adsorbed Pb(II) at the optimum pH of 5.5. The effect of initial Pb(II) concentration (isotherm) shows that the data fitted well with the Langmuir-b isotherm model indicated the monolayer adsorption of Pb(II) onto homogenous surfaces of the HA-UF with the adsorption capacity of 2.26 × 10^{-4} mol/g (which is higher than its original HA of 1.12 × 10^{-4} mol/g). The Ho (pseudo-second-order) kinetics model represented the effect of contact time (kinetics) was represented by the Ho kinetics model. The synthesized adsorbent is also reusable, with 88.59% of adsorption capacity remaining in the fifth recycle run. Therefore, the adsorbent of HA-UF is suggested to be a promising candidate for adsorption applications.*

Keywords: *humic acid-urea formaldehyde (HA-UF); Pb(II) adsorption; pH and ionic strength; isotherm; kinetics studies*

■ INTRODUCTION

According to the World Health Organization (WHO), the heavy metals requiring immediate attention to remove from the environment are Cr, Cd, Zn, Fe, Hg, Co, and Pb [1]. Therefore, removing heavy metals from water or wastewater is a major concern in water treatment. Various methods are reported to reduce heavy metals, such as ionic exchange, electrolysis, membrane separation, chemical precipitation, and adsorption. Of all the methods above, adsorption is considered one of the simplest and most effective techniques [2]. To date, various effective adsorbents such as activated carbon [3], humic acid (HA) [4], MWCNTs [5], γ-alumina [5], chitosan-coated Fe_3O_4 [6], granular ferric hydroxide [7],

and urea-formaldehyde (UF) [8] have been reported in the literature.

Recently, HA has been widely utilized to reduce heavy metals, pigments, radioactive and organic pollutants in water. HA contains various functional groups involved in the binding and entrapment of metal ions. In addition, HA is economically affordable, eco-friendly, abundant sources, and does not cause secondary pollution. Although it possesses many promising properties, natural HA is easy to dissolve in an alkaline medium, reducing its performance as an adsorbent. Previous works have successfully modified HA with chitin or chitosan [9], magnetite [10], titanium dioxide [11], Ca-montmorillonite [12], attapulgite [13], starch [14], and carboxymethylcellulose (CMC) [15], to achieve HA-based high-performance adsorbent. As reported in the literature, the requirements of HA modifiers are relatively stable at high pH, low cost, high availability, and abundant functional groups materials. One of the materials that possess these properties, but no publication reported it as HA modifier, is urea-formaldehyde (UF).

UF is a low-cost polymeric condensation product of urea and formaldehyde, consisting of [–CH_2–NH–CO–NH–CH_2–] repeating units. UF is rich in amine, amide, hydroxyl, and carbonyl groups which can interact with many metal ions in an aqueous solution through a complexation mechanism. Other researchers have previously reported the study of UF as an adsorbent for heavy metal ions [8,16-19]. The study results showed that UF adsorbent could efficiently remove highly concentrated heavy metal ions from aqueous solutions. However, no publications were found investigating HA-UF as a heavy metal adsorbent. In contrast, the modification of HA by UF can enhance an HA-based adsorbent with high stability, low cost, and high performance.

This study aims to investigate the formation of HA-UF and the adsorption performances of HA-UF in three aspects, i.e., the effect of pH and ionic strength, initial concentration (isotherm study), and contact time (kinetics study). Pb(II) was selected as the adsorbate model for evaluating HA-UF performance because of its toxic properties and wide application in food cane solders, ceramic glaze, batteries, cosmetics, and mining industries [20]. Further, the reusability of the HA-UF as Pb(II) adsorbent was also investigated in this work.

■ EXPERIMENTAL SECTION

Materials

HA was extracted from 100 mesh dry peat soil powder of Indragiri Hilir, Riau, Indonesia. The extraction and the purification of HA were performed by the IHSS (International Humic Substance Society) method. The urea used in this study was commercial urea which is available in Yogyakarta. All reagents were pro analyst grade, i.e., formaldehyde solution 37%, NaOH pellet, HCl fuming 37%, HF solution 48%, HNO_3 solution 65%, CH_3COOH glacial 100%, $Ba(OH)_2$ powder, $Pb(CH_3COO)_2{\cdot}2H_2O$ powder, and NaCl powder produced by Merck® and they are used without further purifications.

Procedure

Preparation of the adsorbent

Five grams of urea were dissolved in 14 mL of 37% formaldehyde (mole ratio = 1:2). After 3 min of stirring, dissolved HA (5 g) was added in 200 mL of NaOH 0.1 M. The mixture was stirred and refluxed for 4 h at 75 °C. The mixture was then cooled to room temperature and neutralized by adding HCl 2.5 M dropwise. The mixture was separated by 3950 rpm centrifugation for 10 min to obtain sediment (the sediment was a dark brown solid, and the filtrate was a yellow liquid). The solid was washed with distilled water and dried at 60 °C as HA-UF dry adsorbent. HA-UF was characterized with Attenuated Total Refection-IR (ATR-IR Thermo Scientific Nicolet iS50 at 400–4000 cm^{-1} wavenumber), XRD (PANalytical X'pert PRO MRD with Ni-filtered Cu Kα radiation as the X-Ray source between 2θ = 3°–90°), and SEM-EDX (Analysis Phenom-World JSM 6510LA-Phenom world Analysis).

Properties of synthesized adsorbent

The difference of total acidity also carried out HA-UF properties, pH point of zero charges (pH_{PZC}), and stability at varied pH with the original HA as a comparison. The Baryta indirect potentiometric titration method was determined by the total acidity of HA-UF

and HA. The pH_{PZC} was conducted by dissolving 50 mg of sample (HA-UF and HA) in 25 mL of distilled water with a pH range of 2.0–11.0. The mixture was shaken at 250 rpm for 1 h and aged for 48 h. The pH_{PZC} was identified by plotting the initial pH vs. the final and initial pH difference (ΔpH). The stability of the adsorbent was carried out by dissolving 0.1 g of each sample in distilled water with a pH range of 1.0–14.0 in different test tubes. After 24 h stirring, the remaining solids were weighed, and the percentage was calculated as the stability of the adsorbent.

Effect of medium acidity and ionic strength

A series of 20 mL of Pb(II) 20 mg/L at adjusted pH by adding HCl and NaOH solution ranging from 2.2–8.8 was prepared. Into each of the prepared solutions, 50 mg of HA-UF was added. After 3 h of shaking by 250 rpm, the mixture was filtered, and the filtrate was analyzed with Flame-AAS (Perkin Elmer 3110) to obtain adsorbed Pb(II). The highest adsorbed Pb(II) was clearing as the optimum pH.

The effect of ionic strength was carried out in two aspects: pH_{PZC} of adsorbent and Pb(II) adsorption. The effect of ionic strength on the pH_{PZC} adsorbent was conducted by a similar procedure to determine pH_{PZC}. However, NaCl was added to each sample so that the final concentration of NaCl was 0.1 M. The effect of ionic strength on Pb(II) adsorption was studied by preparing a 5 series of 20 mL of Pb(II) 20 mg/L at optimum pH. NaCl was added to the solution so that the final concentrations of NaCl were 0.1, 0.2, 0.3, 0.4, and 0.5 M. After 3 h shaking at 250 rpm, the mixture was filtered, and the filtrate was analyzed with Flame-AAS to measure the adsorbed Pb(II).

Every sample was accompanied by a blank solution containing no HA-UF adsorbent, and both of them were treated under identical conditions. The amount of Pb(II) adsorbed into the HA-UF was considered to be the difference between the initial (blank solution) and the remaining amount of Pb(II) in the sample.

Isotherm and kinetic adsorption experiments

The isotherm experiments were carried out by contacting the adsorbent with Pb(II) at various concentrations. Fifty milligrams of adsorbent were interacted with 20 mL of Pb(II) solutions with various concentrations (5, 10, 20, 30, 40, 60, 80, 100, 150, and 200 mg/L) at optimum pH. After 180 min of 250 rpm shaking, the mixture was filtered, and the filtrate was analyzed with Flame-AAS.

The kinetics experiments were carried out by contacting 50 mg adsorbent with 20 mL of Pb(II) 20 mg/L at different contact times (10, 20, 30, 50, 60, 90, and 180 min). A similar procedure was also performed with different initial concentrations of Pb(II) (50 and 100 mg/L). After being shaken at 250 rpm at a determined contact time, the mixture was filtered, and the Pb(II) concentration in the filtrate was analyzed with Flame-AAS.

Every sample was accompanied by a control solution containing no HA-UF adsorbent indicating Pb's actual initial concentration (II). Under the same condition as a sample solution, a control solution was also analyzed. The amount of Pb(II) adsorbed into the HA-UF was considered to be the difference between the initial (control solution) and the remaining amount of Pb(II) in the sample.

Error analysis

Six error functions of average relative error (ARE), sum squares errors (SSE), hybrid fractional error function (HYBRID), sum of absolute error (EABS), nonlinear chi-square test (χ^2), and standard deviation of relative errors (S_{RE}) were applied to evaluate the match of the linear and nonlinear adsorption isotherm (and kinetics) parameters [21]. These error functions estimate the deviation between the experimental data and parameters values predicted by the isotherm models. Six error functions are expressed, as follows:

$$\text{ARE} = \frac{100}{x}\sum_{i=1}^{x}\left|\frac{q_{e,means} - q_{e,calc}}{q_{e,means}}\right| \quad (1)$$

$$\text{SSE} = \sum_{i=1}^{x}(q_{e,calc} - q_{e,means})_i^2 \quad (2)$$

$$\text{HYBRID} = \frac{100}{x-p}\sum_{i=1}^{x}\left[\frac{q_{e,means} - q_{e,calc}}{q_{e,means}}\right] \quad (3)$$

$$\text{EABS} = \sum_{i=1}^{x}\left|q_{e,means} - q_{e,calc}\right| \quad (4)$$

$$\chi^2 = \sum_{i=1}^{x}\frac{(q_{e,calc} - q_{e,means})^2}{q_{e,means}} \quad (5)$$

$$S_{RE} = \sqrt{\frac{\sum_{i=1}^{x}\left[\left(qe,means - qe,calc\right)_i - ARE\right]^2}{x-1}} \quad (6)$$

where $q_{e,means}$ and $q_{e,calc}$ are measured adsorbed Pb(II) from isotherm model (mg/g) and calculated adsorbed Pb(II) at equilibrium (mg/g), respectively.

The performance of the error function for the approximation of adsorption isotherm parameters can be evaluated using the procedure of normalizing and combining the error results to determine the Sum of Normalized Errors (SNE). After the SNE values for each parameter set are compared, the model provided the lowest SNE value is considered the most relevant result.

Reusability

A reusability study of HA-UF was carried out by performing the five consecutive cycles of the adsorption-desorption runs. Adsorption of Pb(II) onto HA-UF was conducted by contacting 50 mg of HA-UF with 25 mL of Pb(II) 20 mg/L at optimum pH. After 60 min of 250 rpm shaking, HA-UF loaded Pb(II) was filtered, and the filtrate solution's pH was measured. A control solution containing no HA-UF adsorbent was also prepared, indicating the actual initial concentration of Pb(II). The desorption of adsorbed-Pb(II) on HA-UF was performed by conducting HA-UF loaded Pb(II) with 25 mL of three different eluents: HCl 0.01 M, HNO_3 0.01 M, and CH_3COOH 0.01 M. After 60 min shaking at 250 rpm, the HA-UF released Pb(II) was filtered and washed with deionized water until pH neutral. The process was repeated for five consecutive cycle runs. The adsorption and desorption process filtrate was analyzed with Flame-AAS to quantify absorbed and desorbed Pb(II), respectively. The amount of Pb(II) adsorbed into the HA-UF was considered to be the difference between the initial (control solution) and the remaining amount of Pb(II) in the filtrate. The amount of Pb(II) desorbed from the HA-UF was considered to be the difference between the adsorbed Pb(II) and desorbed Pb(II) in the filtrate.

■ RESULTS AND DISCUSSION

Characterization of HA-UF

The characteristic band of urea using ATR-IR at wavenumber 1690 cm^{-1} was attributed to the C=O amide stretching, 3310 cm^{-1} could be assigned to secondary amine N–H stretching, and between 1250–1020 cm^{-1} was designated for amide C–N stretching (Fig. 1(a)) [22]. In addition, the sharp bands at 1585 and 1453 cm^{-1} were associated with the N–H bonds and fewer characteristics of C–O–H due to the aliphatic side groups of the amino acid residues in commercial urea [23], respectively.

The peaks between 2830–2695 cm^{-1} referred to the C–H aliphatic stretching, and at 1655 cm^{-1} referred to the aldehyde C=O stretching, which was characteristic spectra of formaldehyde (Fig. 1(a)) [18]. Five characteristic bands of HA were displayed at 3300–3400 cm^{-1} (attributed to O–H and N–H stretching), 2918 cm^{-1} (designated for C–H aliphatic stretching), 1715 cm^{-1} (referred to C=O from carboxylic acid stretching), 1620 cm^{-1} (assigned to aromatic C=C stretching), and 1236 cm^{-1} (attributed to C–O from ester stretching) (Fig. 1(b)).

ATR-IR spectrum of the UF prepared by the reflux method is shown in Fig. 1(a). Important broadband around 3650–3000 cm^{-1} can be attributed to the hydrogen-bonded O–H and N–H, and its broadness might be due to water and formaldehyde monomers. This O–H group of water and formaldehyde of UF may form hydrogen bonds with reactive functional groups such as CH_2OH, NH_2, and NH [22]. The small band in the region of 2920 cm^{-1} is the C-H stretching vibrations of UF. The overlapped peak at 1720 cm^{-1} is related to C=O stretching. The two peaks area at the 1500–1600 cm^{-1} are attributed to –N–H bending vibrations of secondary amide. A relatively intense and broad peak at 1236–1249 cm^{-1} is assigned to C–N stretching vibrations of secondary amide. Finally, the quietly strong peak at 1017 cm^{-1} is due to the C–C–O stretching mode of CH_2OH [24].

The success of HA-UF synthesis characterized with ATR-IR can be seen from the combination peak of original urea, formaldehyde, and HA as a constituent of HA-UF in HA-UF spectra, i.e., emerging peak between 1250–1020 cm^{-1} was ascribed to the C–N stretching of amide III (Fig. 1(a)) [22]. This emerging peak leads to the notion that the formation of HA-UF occurred through

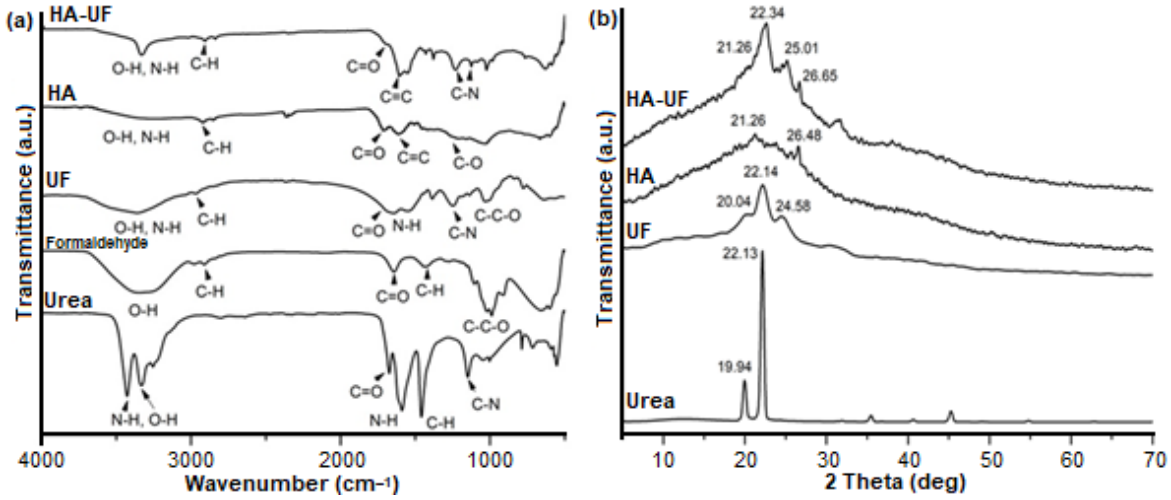

Fig 1. (a) ATR-IR spectra of HA-UF, HA, UF, formaldehyde, and urea; (b) XRD Diffractogram of urea, HA, UF, and HA-UF

C–N bonding. This fact is due to an increase in the intensity of C–N stretching at 1236 cm^{-1} in HA-UF spectra (Fig. 1(a)).

Fig. 1(b) presents the X-ray diffractograms of urea, HA, UF, and HA-UF. As shown, urea exhibited a high crystalline order with double sharp peaks at 2θ = 19.94° and 22.23°. The peak at 2θ around 22° was ascribed to (002) interlayer reflection of urea [25-26]. The UF diffractogram showed three sharp, strong 2θ peaks at 20.04°, 22.14°, and 24.58°. The first two peaks indicate the urea crystal, and the apparent additional peak (24.58°) is the typical peak on the XRD diffractogram of pure UF composites [17]. It was also observed that the position of the peak at 2θ = 19.94° (urea) shifted right to 20.04° (UF), probably due to the small urea that could intercalate into the UF composite interlayer [27]. The increasing crystallinity measurement from 54.09% (urea) to 76.59% (UF) strengthened the successful formation of UF. In contrast to urea, HA exhibited no specific sharp peak with high intensity due to the amorphous material [25-26], as demonstrated by XRD analysis [28]. Compared to UF, HA-UF occurred decreasing in crystallinity to 51.75% due to fairly semi-crystalline as it appears at 2θ around 22° and 25°. Hence, the measured reduction in the crystallinity of HA-UF is related to the amorphous structure of HA.

The results of the cross-sectional SEM analysis are displayed in Fig. 2 that represents the morphology of HA, UF, and HA-UF by magnifying 5000 times from the original image size. Arshad et al. [22] reported that different phases of UF presented in the SEM micrograph were identified using their differences in colors and contrasts. Related to that, the SEM micrograph in Fig. 2(b) broadly depicts two different phases in HA-UF due to their color contrast. However, the distribution of these phases is fairly homogeneous and similar. Supporting these findings, elemental composition analysis with EDX showed an increase in the N atoms in HA-UF (23.46%, Table 1) from HA. Further, the elemental composition of HA-UF seems the average combination of the elemental composition of HA and UF. These results ascertain that there are two phases of HA and UF that occur, and the UF contains N atoms that truly bind to HA.

The stability of HA-UF compared to HA is presented in Fig. 3. As shown, the synthesized HA-UF started to dissolve at pH 12.0, whereas HA was dissolved at a pH greater than 5.0. The increased stability of HA-UF indicates that the formation of HA and UF involves covalent bonds. The decrease in the total acidity of HA (549.26 cmol/kg) compared with HA-UF (349.30 cmol/kg), the bonds of HA and UF are strongly presumed by the carboxylic group of HA with the nitrogen atom in the UF molecules. This hypothesis follows the increased intensity of C–N stretching at 1236 cm^{-1} in the HA-UF spectra (Fig. 1(a)). This carboxylic group bonding contributes to an increase in pH_{PZC} of HA

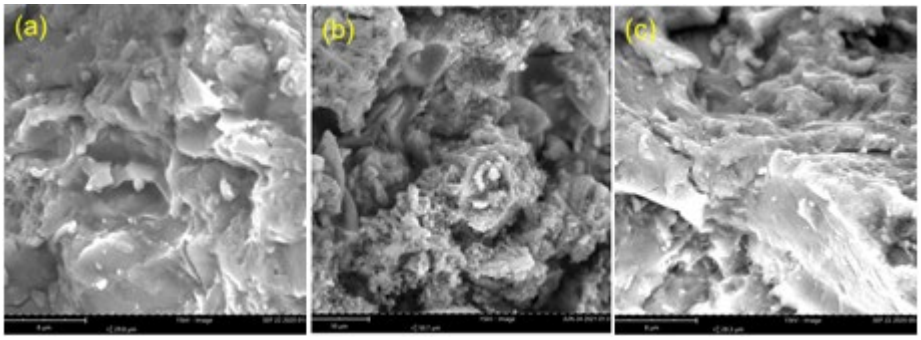

Fig 2. Morphology analyses by SEM-EDX of (a) HA, (b) UF, and HA-UF

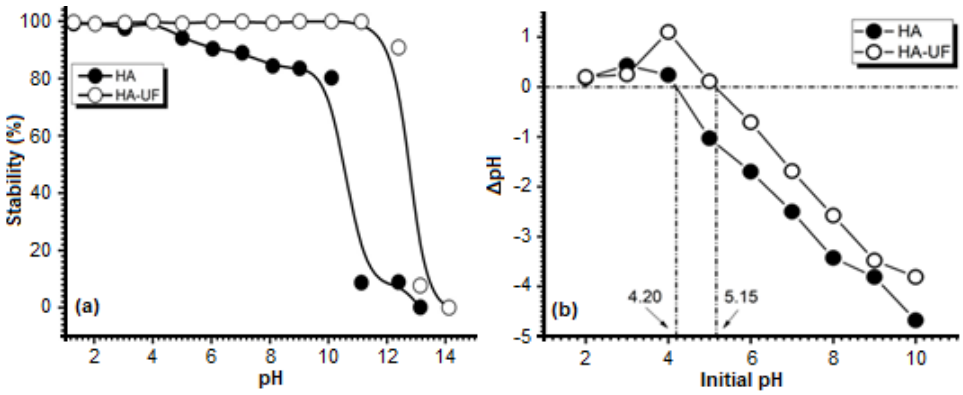

Fig 3. Comparative analysis of the stability (a) and the pH_{PZC} (b) of HA and HA-UF

Table 1. Elemental weight (%) of HA, UF, and HA-UF by EDX

Element	Weight (%)		
	HA	UF	HA-UF
Carbon	57.60	28.56	46.13
Oxygen	35.55	24.38	30.23
Nitrogen	6.860	47.06	23.46

(Fig. 3(b)). The higher the $pH_{PZC,}$ the lower the negatively surface charges [16,25].

From these results, the proposed mechanism for HA-UF formation is presented in Fig. 4. The reflux process accelerates the reaction by heating without reducing the volume of the reacting substance at a temperature of 70–80 °C to prevent swelling of HA and hydrolysis of ammonia carboxylates. The reaction occurs under alkaline conditions to activate the carboxylic ion in the HA. The electrostatic interaction between carboxylic ions and ammonia leads to the

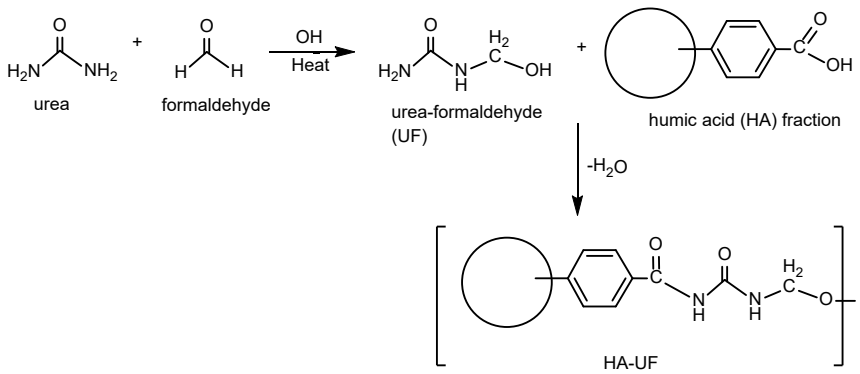

Fig 4. Proposed mechanism of HA-UF formation

formation of ammonium salts due to the low reactivity of carboxylate ions toward addition-elimination of the nucleophile. The further reaction will evaporate water as a dehydration reaction to produce amides. Ammonia salt will efficiently hydrolyze both acidic and alkaline conditions. The precipitation of HA-UF was obtained by acidifying the mixture with the addition of HCl.

Effect of Medium pH and Ionic Strength

The effect of medium pH on Pb(II) adsorption on HA-UF is shown in Fig. 5(a). The adsorbed Pb(II) increases with the increasing pH from 2.0 to 5.0. In this condition, the surface of HA-UF begins to deprotonate, with the result that the HA-UF surface is negatively charged. Hence, Pb^{2+} species will easily be attracted to the HA-UF surface. At high acidity (pH < 3.0), the protonation occurs and competes with Pb^{2+} species to be attracted onto the HA-UF surface. Protonation causes the HA-UF surface to be zero/positively charged, leading to inactivity/repulsion between Pb^{2+} species and active sites of HA-UF. Therefore, Pb(II) adsorption is low on HA-UF is low under low pH conditions. The highest Pb(II) adsorption on HA-UF was obtained at a pH above 5.0 (Fig. 5(a)). However, at pH approximately above 6.0, the formation of solid $Pb(OH)_2$ initially began. Thus, high Pb(II) adsorption at pH > 6.0 is not due to Pb(II) being adsorbed onto HA-UF, but it is Pb(II) precipitated as solid $Pb(OH)_2$. Considering the existence of Pb^{2+} species and the formation of solid $Pb(OH)_2$, the optimum pH of Pb(II) adsorption onto HA-UF was achieved between pH 5.0 and 6.0. As illustrated in Fig. 5(a), it can also be seen that the maximum adsorption value of Pb(II) on HA-UF was obtained at initial pH > pH_{PZC}. Therefore, electrostatic attractions between negatively charged surfaces of the HA-UF and Pb^{2+} species can occur and contribute to adsorption. Previous findings in the adsorption of Pb(II)

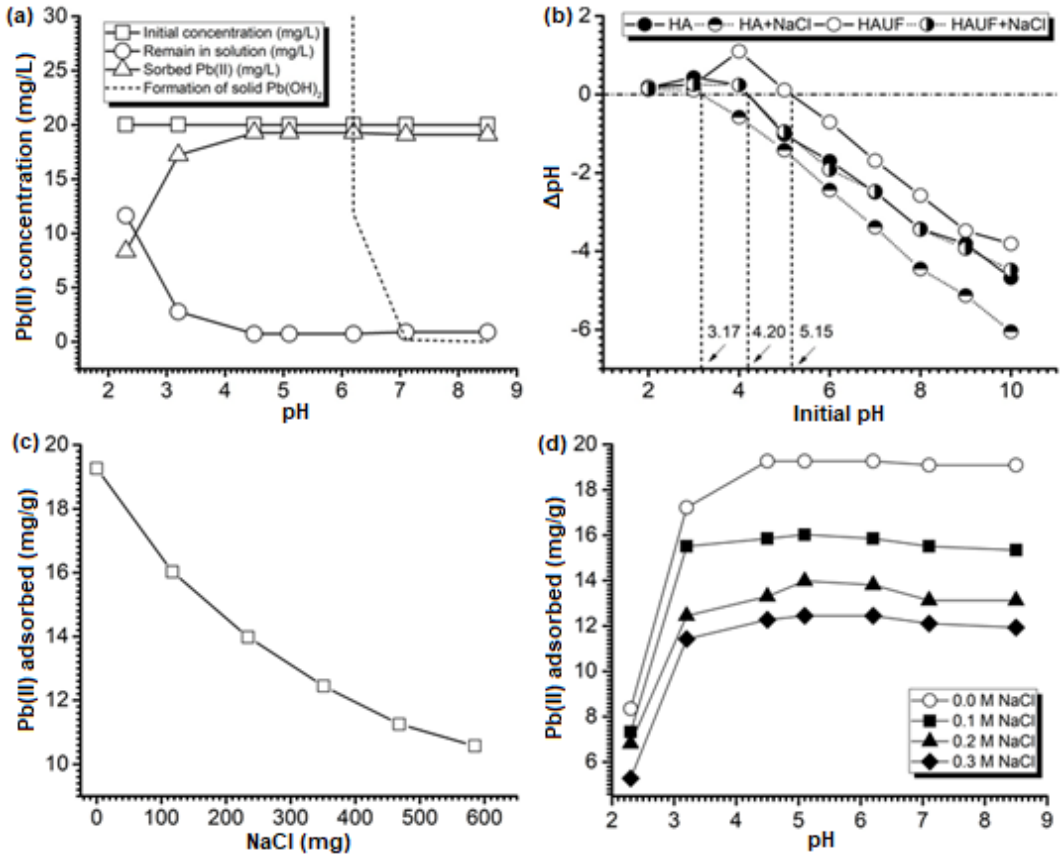

Fig 5. (a) Profile of Pb(II) adsorption onto HA-UF as a function of pH, (b) Effect of the 0.1 M NaCl presence to the pH_{PZC} of HA and HA-UF, (c) Effect of the NaCl salt addition to the adsorbed Pb(II) onto HA-UF at pH 5.50, (d) Profile of Pb(II) adsorption onto HA-UF as a function of pH in the NaCl presence (20 mL of Pb(II) 20 mg/L, 50 mg HA-UF)

onto HA-based adsorbents showed similar results to this work: an optimum pH of 5.0 in peat-HA [28], and an optimum pH of 5.5 in a magnetite/HA/chitosan adsorbent [10].

The effect of the ionic strength with the addition of NaCl to pH_{PZC} is presented in Fig. 5(b). The pH_{PZC} of HA and HA-UF decreased 4.2–3.17 and 5.15–4.2, in the presence of 0.1 M NaCl, respectively (Fig. 5(b)). A decrease in pH_{PZC} indicates that the HA and HA-UF surfaces' zero-point charge occurs at stronger acidic conditions (more H^+ ions). It means that additional H^+ is needed to enhance Cl^- from the addition of NaCl in the solution. The result is that there are more H^+ ions in the solution than on the adsorbent surface, so that the adsorbent surface is negatively charged in a more acidic solution.

The effect of the ionic strength with the addition of NaCl on the Pb(II) adsorption is presented in Fig. 5(c). As shown, the higher the concentration of NaCl reduces the adsorption of Pb(II) onto HA-UF. The low adsorption of Pb(II) in this work (or other divalent metal cations) has been attributed to different factors: (1) adsorbent active site blocking by salt, (2) repulsion between free positive charge adsorbate and positively charged of adsorbent surfaces, (3) competition between positively charged species (H^+ and Pb^{2+}) and free adsorbate to the sorbent active sites, (4) lower formation of complexes/chelate with metal ions due to protonation of surface functional groups, and (5) combination of several of these factors [29]. The presence of NaCl has been observed to cause a decrease in adsorbed Pb(II) onto HA-UF (Fig. 5(d)). The sorption of Pb(II) on HA-UF is influenced by ionic strength at pH < 4.50, whereas no drastic difference of Pb(II) adsorption was found at pH > 4.50 in three different NaCl concentrations. The results presented in Fig. 5(c) and 5(d) showed that the adsorption of Pb(II) onto HA-UF seems to be affected by the first and third factors because even at the optimum pH (5.50) and the optimum pH > pH_{PZC}, the Pb(II) adsorption continues to decrease with the increase of ionic strength (NaCl concentration).

Isotherm Adsorption Study

The equilibrium adsorption isotherm is essential in describing the interactive behavior between the adsorbate, Pb(II), and adsorbent, HA-UF. For example, Fig. 6(a) presents Pb (II) adsorbed onto HA and HA-UF with different Pb(II) initial concentrations at an optimum pH of 5.5. The adsorbed Pb(II) increases with an increase of equilibrium concentration of Pb(II), and reaches the saturation plateau. As exhibited, the saturation plateau of HA-UF was higher than that of HA. It is indicated that the adsorption capacity of HA-UF is higher than HA due to modification with UF.

The equilibrium adsorption parameters were obtained from a linear and nonlinear form of four styles Langmuir, Freundlich, Dubinin-Radushkevich (D-R) [30], and Temkin [31] isotherm models (Table 2). The nomenclatures of the symbols are b (mg/g or mol/g), which represent is the monolayer adsorption capacity, q_e (mol/g) denote Pb(II) adsorption on the adsorbent at equilibrium, K_L (L/mol) is Langmuir equilibrium constant, E_L (kJ/mol) is the monolayer adsorption energy [E_L=-RT ln K_L], C_0 and C_e are Pb(II) initial concentration (mol/L) and remains Pb(II) concentration at equilibrium (mol/L), respectively. The B (mg/g or mol/g) is the multilayer adsorption capacity, n is the heterogeneity parameter of the adsorbent surface, β is Dubinin-Radushkevich (D-R) isotherm constant (mol^2/kJ^2), ε is Polanyi potential [RT In(1+1/C_e)] (J^2/mol^2), q_{D-R} (mol/g) is the theoretical isotherm saturation capacity, b_T (J/mol) and A_T (L/g) are Tempkin isotherm parameters, R (8.314 J/mol K) is the gas constant, and T is the absolute temperature. The closest correlation coefficient (R^2) to the unity among the Langmuir styles and the three other models were then evaluated by a six error function (Eq. (1–6)) to compare the linear and nonlinear adsorption fitness isotherm parameters.

The plot of experimental data to the four styles of Langmuir, Freundlich, D-R, and Temkin models is presented in Fig. 6(b–h). From the plot among Langmuir linear model (Fig. 6(b–e)), the Langmuir-b shows the highest value of R^2 (Fig. 6(c)). The adsorption isotherm parameters value and the calculated error value were listed in Table 3. For the linear regression method, the Langmuir isotherm emerged to be the most appropriate model for the adsorption of both HA and HA-UF due to the higher R^2 value. In the nonlinear

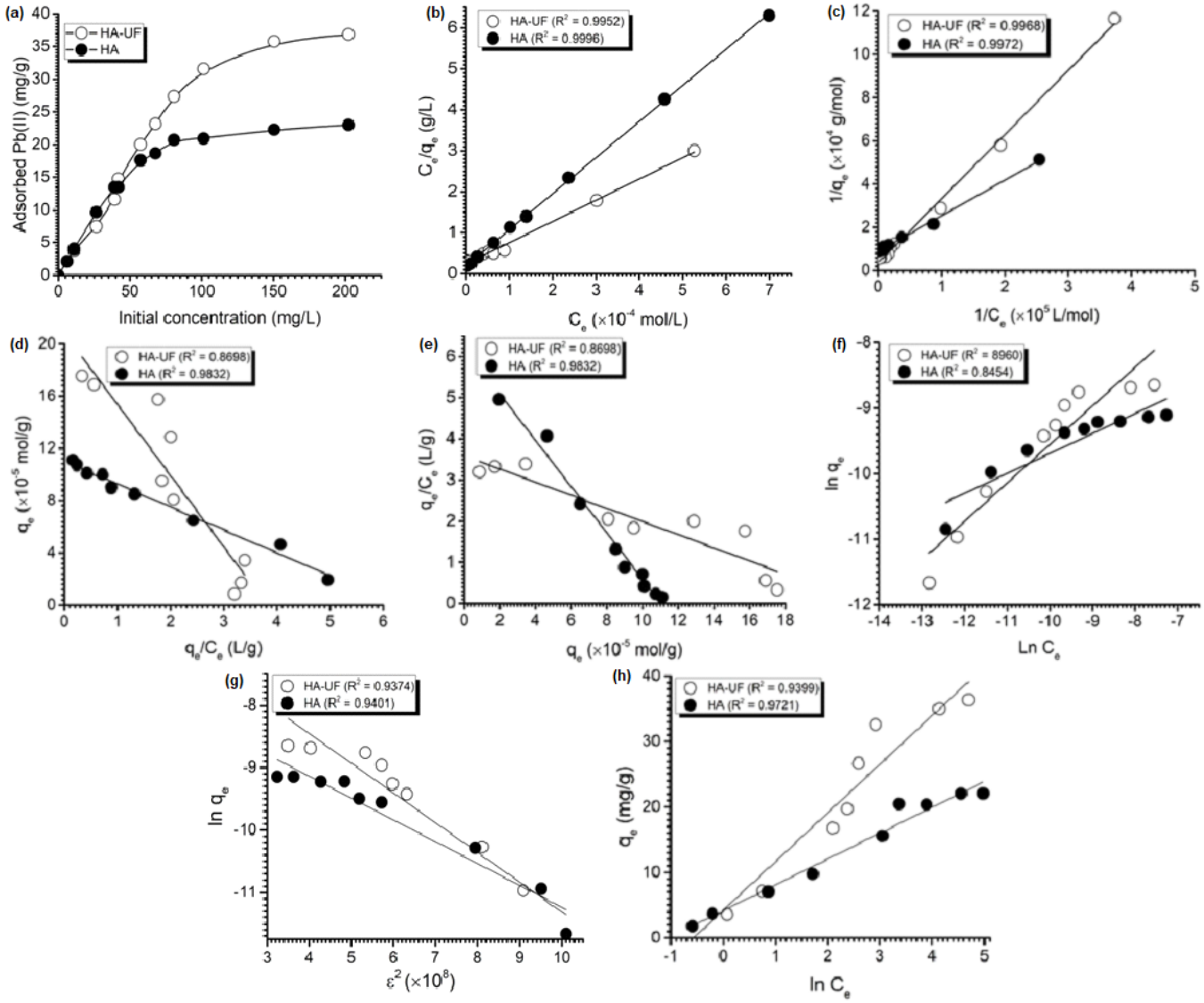

Fig 6. (a) Effect of Pb(II) initial concentration to the adsorbed Pb(II) onto HA and HA-UF; the plot of isotherm experimental data to the (b) Langmuir-a; (c) Langmuir-b; (d) Langmuir-c; (e) Langmuir-d; (f) Freundlich; (g) D-R; and (h)Temkin linear form model

method, the Freundlich isotherm presented lower error values than other nonlinear isotherm models for both HA and HA-UF adsorbents. However, the Freundlich isotherm parameter sets obtained from the nonlinear model differed from the linear regression value.

Conversely, several Langmuir-a isotherm parameter sets generated from the nonlinear regression were similar to the linear regression values. Among the isotherm parameter sets are determined using nonlinear regression. It was noticed that the isotherm parameter sets derived by ARE and S_{RE} were similar. In order to choose the appropriate isotherm parameter set, the sum of normalized errors (SNE) was considered. The SNE was calculated by dividing the error values by the maximum error of that error function. The parameter set yielded the smallest SNE value was proclaimed as the appropriate parameter set. As seen in Table 3, the lowest SNE was obtained from the Langmuir-a parameter set for both HA and HA-UF adsorbents. It means that the Langmuir-a isotherm model assigned the match close to the experimental data.

Table 2. Linear and nonlinear form of the isotherm models

Isotherm models	Nonlinear form	Linear form	Plot (x vs. y)	Slope	Intercept	Ref.
Langmuir-a	$q_e = \frac{K_L b C_e}{1 + b C_e}$	$\frac{C_e}{q_e} = \frac{1}{K_L b} + \frac{1}{b} C_e$	C_e vs. $\frac{C_e}{q_e}$	$\frac{1}{b}$	$\frac{1}{K_L b}$	[32]
Langmuir-b		$\frac{1}{q_e} = \frac{1}{b} + \frac{1}{b K_L C_e}$	$\frac{1}{C_e}$ vs. $\frac{1}{q_e}$	$\frac{1}{K_L b}$	$\frac{1}{b}$	[32]
Langmuir-c		$q_e = b - \frac{q_e}{K_L C_e}$	$\frac{q_e}{C_e}$ vs. q_e	$\frac{1}{K_L}$	b	[32]
Langmuir-d		$\frac{q_e}{C_e} = K_L b - q_e K_L$	q_e vs. $\frac{q_e}{C_e}$	K_L	$K_L b$	[32]
Freundlich	$q_e = B C_e^{1/n}$	$\ln q_e = \ln B + \frac{1}{n} \ln C_e$	$\ln C_e$ vs. $\ln q_e$	$\frac{1}{n}$	$\ln B$	[33]
D–R	$q_e = (q_{D-R}) \exp(-\beta \varepsilon^2)$	$\ln q_e = \ln q_{D-R} - \beta \varepsilon^2$	ε^2 vs. $\ln q_e$	β	$\ln q_{D-R}$	[30]
Temkin	$q_e = \frac{RT}{b_T} \ln A_T C_e$	$q_e = \frac{RT}{b_T} \ln A_T + \frac{RT}{b_T} \ln C_e$	$\ln C_e$ vs. q_e	$\frac{RT}{b_T}$	$\frac{RT}{b_T} \ln A_T$	[31]

Table 3. Linear regression of adsorption isotherm parameters and error analysis calculation

Models	Adsorbent	Parameter	Linear regression	Nonlinear regression					
				ARE	SSE	HYBRID	EABS	$\chi 2$	S_{RE}
Langmuir-b	HA-UF	b (mg/g)	46.80	46.40	46.40	46.40	46.40	46.40	46.40
		K_L (L/mol)	12143	21884	21884	21884	21884	21884	21884
		E_L (kJ/mol)	23.30	23.30	23.30	23.30	23.30	23.30	23.30
		R^2	0.9968						
		Error value		0.279	2.35×10^{-9}	0.439	6.90×10^{-6}	1.05×10^{-5}	0.279
		SNE	0.378	0.636	5.35×10^{-9}	1.00	1.57×10^{-5}	2.39×10^{-5}	0.635
	HA	b (mg/g)	23.12	37.60	37.60	37.60	37.60	37.60	37.60
		K_L (L/mol)	53507	43961	43961	43961	43961	43961	43961
		E_L (kJ/mol)	23.22	23.33	23.33	23.33	23.33	23.33	23.33
		R^2	0.9996						
		Error value		0.103	3.38×10^{-7}	0.162	2.06×10^{-5}	1.86×10^{-4}	0.102
		SNE	0.378	0.636	2.09×10^{-7}	1.00	1.27×10^{-5}	1.15×10^{-3}	0.633
Freundlich	HA-UF	B (mg/g)	5179	64740	64740	64740	64740	64740	64740
		n	1.71	2.90	2.90	2.90	2.90	2.90	2.90
		R^2	0.8960						
		Error value		0.091	0.010	0.143	0.003	0.034	0.087
		SNE	0.430	0.636	0.075	1.00	0.021	0.240	0.610
	HA	B (mg/g)	414	2736	2737	2737	2737	2737	2737
		n	3.29	5.39	5.39	5.39	5.39	5.39	5.39
		R^2	0.8454						
		Error value		0.092	1.90×10^{-5}	0.145	1.35×10^{-4}	1.44×10^{-3}	0.091
		SNE	0.379	0.636	1.31×10^{-4}	1.00	9.25×10^{-4}	9.89×10^{-3}	0.631

Table 3. Linear regression of adsorption isotherm parameters and error analysis calculation (*Continued*)

Models	Adsorbent	Parameter	Linear regression	Nonlinear regression					
				ARE	SSE	HYBRID	EABS	$\chi 2$	S_{RE}
D-R	HA-UF	qD (mg/g)	438.06	438.06	438.06	438.06	438.06	438.06	438.06
		E_{DR} (kJ/mol)	9.75	9.75	9.75	9.75	9.75	9.75	9.75
		R^2	0.9374						
		Error value		0.110	4.51×10^{-7}	0.174	2.58×10^{-5}	2.13×10^{-4}	0.110
		SNE	0.378	0.636	2.59×10^{-6}	1.00	1.480×10^{-4}	1.22×10^{-3}	0.633
	HA	qD (mg/g)	84.22	84.21	84.21	84.21	84.21	84.21	84.21
		E_{DR} (kJ/mol)	12.55	12.55	12.55	12.55	12.55	12.55	12.55
		R^2	0.9401						
		Error value		0.145	1.29×10^{-8}	0.229	6.52×10^{-6}	3.17×10^{-5}	0.145
		SNE	0.378	0.636	5.62×10^{-8}	1.00	2.84×10^{-5}	1.38×10^{-4}	0.634
Temkin	HA-UF	b_T (J/mol)	319.07	117.99	117.99	117.99	117.99	117.99	117.99
		A_T (L/g)	1.51	1.24	1.24	1.24	1.24	1.24	1.24
		q_e (mg/g)	26.96	68.79	68.79	68.79	68.79	68.79	68.79
		R^2	0.9399						
		Error value		0.218	6.83×10^{-9}	0.343	7.98×10^{-6}	2.06×10^{-5}	0.218
		SNE	0.379	0.636	1.99×10^{-8}	1.00	2.32×10^{-5}	5.99×10^{-5}	0.635
	HA	b_T (J/mol)	640.99	172.41	172.41	172.41	172.41	172.41	172.41
		A_T (L/g)	4.36	1.12	1.12	1.12	1.12	1.12	1.12
		q_e (mg/g)	19.27	52.12	52.12	52.12	52.12	52.12	52.12
		R^2	0.9721						
		Error value		0.179	3.93×10^{-9}	0.281	4.97×10^{-6}	1.56×10^{-5}	0.179
		SNE	0.379	0.636	1.40×10^{-8}	1.00	1.76×10^{-5}	5.54×10^{-5}	0.635

The R_L value of Pb(II) adsorption onto HA and HA-UF in this study shows that the R_L values of HA (0.427–0.022) and HA-UF (0.395–0.019) are between 0 and 1, which indicates the adsorption is a favorable process. It suggests the homogeneity of the HA-UF surface. The adsorption capacity of Pb(II) adsorption onto HA-UF (2.26×10^{-4} mol/g or equal to 46.80 mg/g) is two times higher than that of HA (1.12×10^{-4} mol/g or equal to 23.12 mg/g). Comparison of the adsorption capacity (b) of HA-UF as Pb(II) adsorbent with the HA- or UF-based adsorbents were listed in Table 4. Since the total acidity has decreased from 549.26 cmol/kg (HA) to 349.30 cmol/kg (HA-UF), it can be concluded that Pb(II) adsorption involves the interaction between Pb(II) and the lone pair electron of the N atom in UF. The higher adsorption capacity of HA-UF can be increased in two ways: using HA with higher total acidity and optimizing the polymerization reaction of HA-UF. With the UF polymer, the loss of one site of the HA–COOH group due to the bonding reaction with the UF polymers will be replaced by more than one N containing the lone pair electron in UF that possibly bind to Pb(II).

Table 4. Comparison of adsorption capacity (b) of the HA-UF as Pb(II) adsorbent

HA-/UF-based Adsorbent	b (mg/g)	References
HA-peat (Polland)	82.31	[34]
Magnetite-HDHA	57.64	[10]
HA-UF	46.80	This work
HA-peat (Riau)	23.12	This work
UF-foam	21.50	[35]
HA-soil (India)	19.60	[36]
HA-peat	15.00	[28]
UF-thiourea-bentonite	13.40	[37]
UF-melamine	4.900	[38]

It is frequently studied that D-R adsorption energy (E_{DR}) is useful for investigating the interaction between the adsorbate and the adsorbent. The interaction could be classified as physical interaction (E_{DR} < 8 kJ/mol), ion

exchange mechanism ($8 < E_{DR} < 16$ kJ/mol), and chemisorption that is stronger than ion exchange ($E_{DR} > 16$ kJ/mol) [39]. The values of E_{D-R} calculated in this study were 9.75 kJ/mol (HA-UF) and 12.55 (HA), which indicated that ion exchange is the major interaction involved in the adsorption process. Furthermore, the Temkin isotherm describes the indirect relation of multilayer interaction between the adsorbate and the adsorbent with the adsorption energy of the layer [40]. As seen in Table 3, the b_T of HA-UF (319.07 J/mol) is smaller than HA (640.99 J/mol) that indicates Pb(II) at the outer layer interact stronger with HA's surface than HA-UF surfaces [40].

Kinetics Adsorption Study

The adsorbed Pb(II) calculated by $(C_0-C_t)/(W/V)$ onto HA-UF as a function of time is presented in Fig. 7(a). It is obvious from Fig. 7(a) that the adsorption amount increases rapidly in the first 20 min, and after 20 min slower adsorption occurs and reaches equilibrium at 100 min. Rapid adsorption within the first 20 min indicates a strong electrostatic interaction between the negative sites of HA-UF and the Pb(II) cations. Four kinetics models (Lagergren [41], Ho [42], Santosa [43], and RBS [10,44-46]) (Table 5) were used to explore kinetics parameters of Pb(II) adsorption onto HA-UF. The nomenclatures of the symbols are q_t (mol/g), which represent the amount Pb(II) that was adsorbed at time t (min); x (mol/L) and x_e (mol/L) are the amount of Pb(II) adsorbed on the adsorbent at time t and equilibrium, respectively; X (g/L) in Santosa's kinetics model is w/vmr, where w (g) is the mass of the adsorbent, v (L) is the volume of sorption medium, and m_r: the molar weight of adsorbate; C_b (mol/L) is the concentration of Langmuir capacity (C_b=bw/v); k_{Lag} (min^{-1}), k_{Ho} (g/mol.min), k_s (L/mol.min), k_a (L/mol.min) are the Lagergren, Ho, Santosa, and RBS rate constants, respectively. The application of empirical data to the plot of these four kinetics models is presented in Fig. 7(b-f).

The corresponding linear regression coefficient (R^2) value of the Ho (Pseudo-Second Order) kinetics model is higher than the other three kinetics models (Table 6). Moreover, the calculated q_e (Calc. q_e) value (5.27×10^{-5} mol/g) from the Ho kinetics model agrees well with the experimental q_e (5.05×10^{-5} mol/g) better than that of Lagergren and RBS kinetics models. Thus,

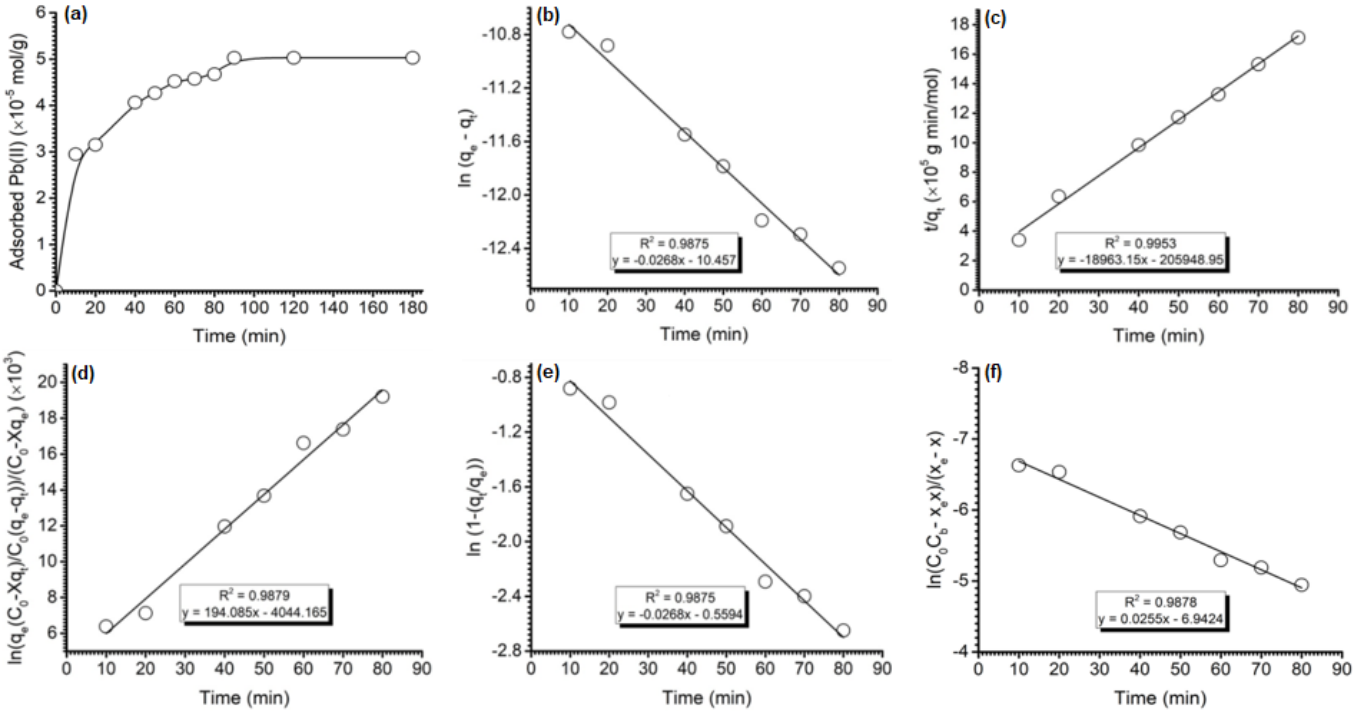

Fig 7. (a) Profile of adsorbed Pb(II) as a function of time; applying of experimental kinetics data to the (b) Lagergren, (c) Ho, (d) Santosa-a), (e) Santosa-b to determine the k_d, and (f) RBS models

Table 5. Kinetics models to determine the kinetics adsorption parameter of HA-UF

Kinetics Model	Linear Form	Plot (*x vs. y*)	Slope	Intercept	Ref.
Lagergren	$\ln(q_e - q_t) = \ln q_e - k_{Lag} t$	t vs. $\ln(q_e - q_t)$	k_{Lag}	$\ln q_e$	[41]
Ho	$\frac{t}{q_t} = \frac{1}{k_{Ho}(q_e^2)} + \frac{1}{q_e} t$	t vs. $\frac{t}{q_t}$	$\frac{1}{q_e}$	$\frac{1}{k_{Ho}(q_e^2)}$	[42]
Santosa	$\frac{1}{C_0 - Xq_e}$ $\ln\left(\frac{q_e(C_0 - Xq_t)}{C_0(q_e - q_t)}\right) = k_s t$	t vs. $\frac{1}{C_0 - Xq_e}$ $\ln\left(\frac{q_e(C_0 - Xq_t)}{C_0(q_e - q_t)}\right)$	k_s	-	[43]
Rusdiarso-Basuki-Santosa (RBS)	$\ln\left(\frac{C_0C_b - x_e x}{x_e - x}\right) =$ $k_a\left(\frac{C_0C_b - x_e^2}{x_e}\right)t - \ln\left(\frac{x_e}{C_0C_b}\right)$	t vs. $\ln\left(\frac{C_0C_b - x_e x}{x_e - x}\right)$	$k_a\left(\frac{C_0C_b - x_e^2}{x_e}\right)$	$\ln\left(\frac{x_e}{C_0C_b}\right)$	[10,44-46]

Table 6. Kinetics parameters of Pb(II) adsorption onto HA-UF

Kinetics Model	Kinetics adsorption parameters				
Lagergren	Calc. q_e (mol/g)	k_{Lag} (min^{-1})	k_d	K	R^2
	2.88×10^{-5}	0.027	-	-	0.9875
Ho	Calc. q_e (mol/g)	k_{Ho} (g mol^{-1} min^{-1})	k_d	K	R^2
	5.27×10^{-5}	1746.04	-	-	0.9953
Santosa	Calc. q_e	k_s ($(mol/L)^{-1}$ min^{-1})	k_{ds} (min^{-1})	K_S $(mol/L)^{-1}$	R^2
	-	194.08	4.46×10^{-5}	4.36×10^{6}	0.9875
RBS	Calc. q_e (mol/g)	k_{RBS} ($(mol/L)^{-1}$ min^{-1})	k_d (min^{-1})	K_{RBS} $(mol/L)^{-1}$	R^2
	1.31×10^{-5}	51.47	2.26×10^{-3}	22780	0.9878

the Ho kinetics model is evidence to demonstrate the adsorption of Pb(II) onto HA-UF. The prediction of adsorption energy through the calculation of E = - RT ln (k_a/k_d) shows that the RBS model (E_{RBS} = 24.86 kJ/mol) presents a closer value than the Santosa model (E_S = 37.87 kJ/mol) to E_L of Langmuir-b (23.30) kJ/mol).

Six different error functions were examined for the nonlinear model of kinetics data (Table 7). The error value of all kinetics models seems to have a different value from the kinetics parameter value calculated from linear regression. However, after being divided by the maximum error (SNE), the lowest value of SNE and the best coherent fitting of the models is for the Ho kinetics model. The SNE value increases in order Ho > RBS > Lagergren. The Santosa kinetics model cannot estimate the error value because the model cannot obtain the $q_{e,calc}$. According to this result, Ho (known as pseudo-second-order) is the best model to represent the kinetics data.

Reusability

Reusability study of HA-UF adsorbent was performed by the five consecutive cycles of the adsorption-desorption process with three different desorption eluents: HCl 0.01 M, CH_3COOH 0.01 M, and HNO_3 0.01 M. The % metal recovery for HA-UF by HCl, CH_3COOH, and HNO_3 after reuse for five consecutive cycles was 90.47%, 67.93%, and 94.32%, respectively. It was observed that the best performance of desorption eluent in this work was HNO_3. A similar result was reported by Basuki et al. [10] in the desorption study of Pb(II) from MHDHA. It might be due to the NO_3^- affinity to make a more stable complex with Pb(II) rather than Cl^- and CH_3COO^- [47].

The pH solution in each adsorption cycle indicates that the pH decreased from the optimum pH (5.50) to 2.91, 3.03, and 2.03 by desorption eluent HCl, CH_3COOH, and HNO_3, respectively, after five consecutive

Table 7. Linear regression of adsorption kinetics parameters and error analysis calculation

Kinetics model	Parameter	Linear regression	Nonlinear regression					
			ARE	SSE	HYBRID	EABS	χ2	MPSD
Lagergren	Calc q_e ($\times10^{-5}$ mol/g)	2.88	6.27	6.27	6.27	6.27	6.27	6.27
	k_{Lag} (min^{-1})	0.027	0.064	0.064	0.064	0.064	0.064	0.064
	k_d	-	-	-	-	-	-	-
	R^2	0.9875						
	Error value		0.310	4.29×10^{-11}	0.516	1.95×10^{-6}	6.84×10^{-7}	0.172
	SNE	0.322	0.600	8.31×10^{-11}	1.00	3.77×10^{-6}	1.32×10^{-6}	0.334
Ho	Calc q_e (mol/g)	5.27×10^{-5}	3.33×10^{12}	3.33×10^{12}	3.33×10^{12}	3.33×10^{12}	3.33×10^{12}	3.33×10^{12}
	k_{Ho} (g mol^{-1} min^{-1})	1746.04	2.70×10^{35}	2.70×10^{35}	2.70×10^{35}	2.70×10^{35}	2.70×10^{35}	2.70×10^{35}
	k_d	-	-	-	-	-	-	-
	R^2	0.9953						
	Error value		1.30×10^{8}	1.92×10^{-10}	2.164×10^{8}	4.33×10^{-6}	577.298	3.029×10^{16}
	SNE	0.166	4.29×10^{-9}	6.35×10^{-27}	7.144×10^{-9}	1.43×10^{-22}	1.91×10^{-14}	1.00
Santosa	Calc q_e	-	-	-	-	-	-	-
	k_s ($(mol/L)^{-1}$ min^{-1})	194.08	-	-	-	-	-	-
	k_{ds} ($\times10^{-5}$ min^{-1})	4.46	-	-	-	-	-	-
	K_s ($\times10^{-6}$ $mol/L)^{-1}$	4.36	-	-	-	-	-	-
	R^2	0.9875	-	-	-	-	-	-
	Error value		-	-	-	-	-	-
	SNE	-	-	-	-	-	-	-
RBS	Calc q_e (mol/g)	1.31×10^{-5}	9.76×10^{-8}	9.76×10^{-8}	9.76×10^{-8}	9.76×10^{-8}	9.76×10^{-8}	9.76×10^{-8}
	k_{RBS} ($(mol/L)^{-1}$ min^{-1})	51.47	2.01×10^{-2}	2.01×10^{-2}	2.01×10^{-2}	2.01×10^{-2}	2.01×10^{-2}	2.01×10^{-2}
	k_d (min^{-1})	2.26×10^{-3}	8.86×10^{-7}	8.86×10^{-7}	8.86×10^{-7}	8.86×10^{-7}	8.86×10^{-7}	8.86×10^{-7}
	K_{RBS} $(mol/L)^{-1}$	22780	22780	22780	22780	22780	22780	22780
	R^2	0.9878						
	Error value		442.322	1.92×10^{-10}	737.20	4.32×10^{-6}	1.96×10^{-3}	3.260×10^{-5}
	SNE	0.167	1.36×10^{-3}	5.88×10^{-16}	2.26×10^{-3}	1.32×10^{-11}	6.02×10^{-9}	1.00

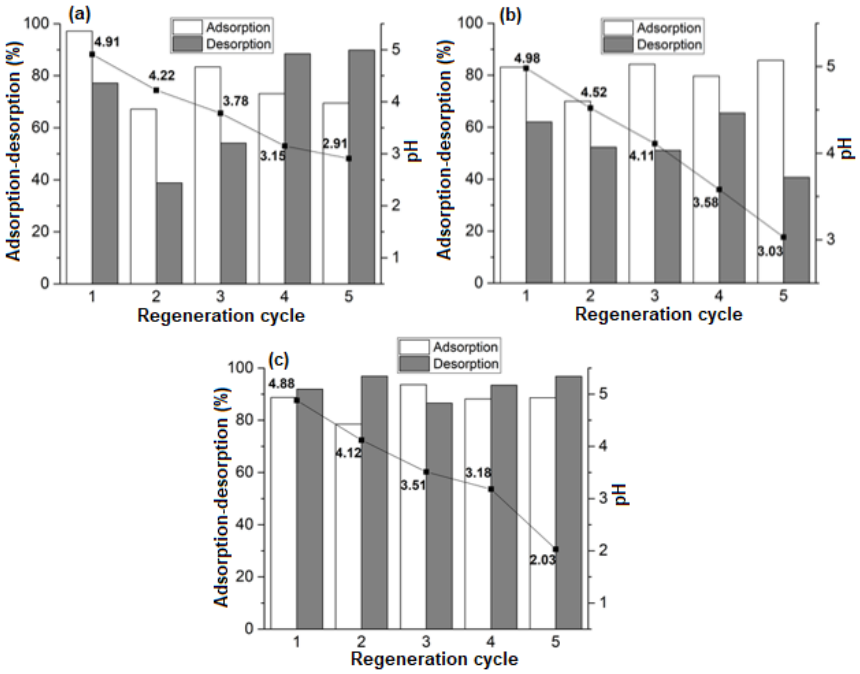

Fig 8. Adsorption-desorption study of HA-UF and pH change in five consecutive cycles with the different eluents: (a) HCl, (b) CH_3COOH, and (c) HNO_3

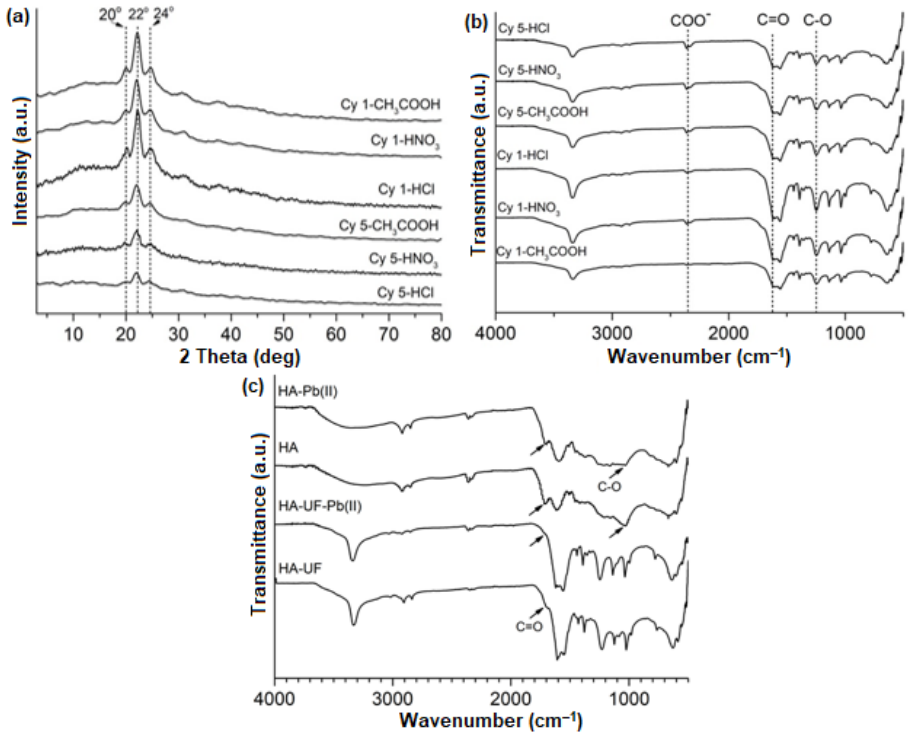

Fig 9. (a) Diffractogram and (b) ATR-IR spectra of HA-UF after the first (Cy1), and fifth cycle (Cy5) adsorption-desorption process with the three different eluents: HCl, CH_3COOH, HNO_3; (c) ATR-IR spectra of HA and HA-UF loaded Pb(II)

adsorption-desorption cycles (Fig. 8). This fact strengthened the calculated E_{D-R} in this work (9.75 kJ/mol) that ion exchange is the main interaction between H^+ of HA-UF surface and Pb(II) ions. Fig. 9(c) showed the interaction Pb(II) with the C=O functional group. At the adsorption process, the H^+ ions were replaced by the Pb(II) ions, and the desorbed H^+ moved into the solution resulting in decreased pH. The H^+ from desorption eluent replaced the adsorbed Pb(II), and the desorbed Pb(II) formed a stable complex with the anion from desorption eluent at the desorption phase.

The five consecutive adsorption-desorption cycles of HA-UF represent the virtuous regeneration ability of HA-UF as an adsorbent. The claim was proved by the XRD and ATR-IR analysis of HA-UF after the fifth adsorption-desorption cycle (Fig. 9). It was observed that there was no significant damage in the crystal system and functional group of the HA-UF. Therefore, the HA-UF offers an efficient, un-expensive, and effective adsorbent for Pb(II) removal from contaminated wastewater.

■ CONCLUSION

The formation of HA-UF and the adsorption performances of the synthesized HA-UF for Pb(II) adsorption were studied. The HA-UF formation was identified as the reaction between the –COOH groups of HA and $–NH_2$ of UF (C–N bonding). The reaction was based on a decrease in the total acidity from 549.26 cmol/kg (HA) to 349.30 cmol/kg (HA-UF), the peak appeared between 1250–1020 cm^{-1} (by ATR-IR), an increase of 23.46% (w/w) N atoms in HA-UF (elemental analysis by EDX), the peaks appeared at 2θ around 22° correspond to (002) interlayer reflection of urea in HA-UF (by XRD) and increased the HA-UF stability in solids form until pH 12.0. The adsorption of Pb(II) onto HA-UF was strongly affected by ionic strength and pH. The higher the ionic strength by adding NaCl salt, the lower the Pb(II) adsorbed at the optimum pH of 5.50. The adsorption isotherm data as the effect of initial Pb(II) concentration variation and its error analysis was fitted well to the Langmuir-b model,

illustrating monolayer ion-exchange adsorption (EDR = 9.75 kJ/mol) on the homogenous surfaces with an average capacity of 2.26×10^{-4} mol/g (equal to 46.80 mg/g). The results of time variation analysis showed that the adsorption followed the Ho (Pseudo-Second order) kinetics model with the rate constant 1746.04 g mol^{-1} min^{-1} and the comparable value of $q_{e,calc}$ (5.27×10^{-5} mol/g) with the experimental $q_{e,exp}$ (5.05×10^{-5} mol/g). The reusability study of HA-UF shows the remarkable performance of up to 95% metal recovered after five consecutive adsorption-desorption cycles by the HNO_3 desorption agent. Therefore, the HA-UF is a promising adsorbent for Pb(II) adsorption in wastewater treatment.

■ ACKNOWLEDGMENTS

The authors thank the Universitas Gadjah Mada for financing this wok through the RTA 2020 Programs (Grant Number: 607/UN1/DITLIT/DIT-LIT/PT/2020).

■ AUTHOR CONTRIBUTIONS

Author 1 conducted the experiments; authors 2 and 3 conceived the theory, formulated the methodology, sourced and presented the data. Authors 1, 2, and 3 prepared and edited the manuscript. The results were reviewed and commented on by all of the authors. All authors agreed with the final version of this manuscript.

■ REFERENCES

[1] Dehghani, M.H., Heibati, B., Asadi, A., Tyagi, I., Agarwal, S., and Gupta, V.K., 2015, Reduction of noxious Cr (VI) ion to Cr (III) ion in aqueous solutions using H_2O_2 and UV/ H_2O_2 systems, *J. Ind. Eng. Chem.*, 33, 10–13.

[2] Siyal, A.A., Shamsuddin, M.R., Rabat, N.E., Zulfiqar, M., Man, Z., and Low, A., 2019, Fly ash based geopolymer for the adsorption of anionic surfactant from aqueous solution, *J. Cleaner Prod.*, 229, 232–243.

[3] Heidarinejad, Z., Dehghani, M.H., Heidari, M., Javedan, G., Ali, I., and Sillanpää, M., 2020, Methods for preparation and activation of activated carbon: A review, *Environ. Chem. Lett.*, 18 (2), 393–415.

[4] Santosa, S.J., Kunarti, E.S., Aprilita, N.H., Wulandari, B., and Bawani, D.N., 2019, Sorption mechanism and performance of peat soil humin for methylene blue and *p*-nitrophenol, *Indones. J. Chem.*, 19 (1), 198–210.

[5] Dehghani, M.H., Yetilmezsoy, K., Salari, M., Heidarinejad, Z., Yousefi, M., and Sillanpää, M., 2020, Adsorptive removal of cobalt(II) from aqueous solutions using multi-walled carbon nanotubes and γ-alumina as novel adsorbents: Modelling and optimization based on response surface methodology and artificial neural network, *J. Mol. Liq.*, 299, 112154.

[6] Rasoulzadeh, H., Dehghani, M.H., Mohammadi, A.S., Karri, R.R., Nabizadeh, R., Nazmara, S., Kim, K.H., and Sahu, J.N., 2020, Parametric modelling of Pb(II) adsorption onto chitosan-coated Fe_3O_4 particles through RSM and DE hybrid evolutionary optimization framework, *J. Mol. Liq.*, 297, 111893.

[7] Shams, M., Nodehi, R.N., Dehghani, M.H., Younesian, M., and Mahvi, A.H., 2010, Efficiency of granular ferric hydroxide (GFH) for removal of fluoride from water, *Fluoride*, 43 (1), 61–66.

[8] Dehghani, M.H., Tajik, S., Panahi, A., Khezri, M., Zarei, A., Heidarinejad, Z., and Yousefi, M., 2018, Adsorptive removal of noxious cadmium from aqueous solutions using poly urea-formaldehyde: A novel polymer adsorbent, *MethodsX*, 5, 1148–1155.

[9] Rusdiarso, B., and Basuki, R., 2020, Stability improvement of humic acid as sorbent through magnetite and chitin modification, *J. Kim. Sains Apl.*, 23 (5), 152–159.

[10] Basuki, R., Rusdiarso, B., Santosa, S.J., and Siswanta, D., 2021, Magnetite-functionalized horse dung humic acid (HDHA) for the uptake of toxic lead(II) from artificial wastewater, *Adsorpt. Sci. Technol.*, 2021, 5523513.

[11] Chen, Q., Yin, D., Zhu, S., and Hu, X., 2012, Adsorption of cadmium(II) on humic acid coated titanium dioxide, *J. Colloid Interface Sci.*, 367 (1), 241–248.

[12] Wu, P., Zhang, Q., Dai, Y., Zhu, N., Dang, Z., Li, P., Wu, J., and Wang, X., 2011, Adsorption of Cu(II), Cd(II) and Cr(III) ions from aqueous solutions on humic acid modified Ca-montmorillonite, *Geoderma*, 164 (3), 215–219.

[13] Zhang, X., Lei, Q., Wang, X., Liang, J., Chen, C., Luo, H., Mou, H., Deng, Q., Zhang, T., and Jiang, J., 2019, Removal of Cr(III) using humic acid-modified attapulgite, *J. Environ. Eng.*, 145 (6), 04019028.

[14] Chen, R., Zhang, Y., Shen, L., Wang, X., Chen, J., Ma, A., and Jiang, W., 2015, Lead(II) and methylene blue removal using a fully biodegradable hydrogel based on starch immobilized humic acid, *Chem. Eng. J.*, 268, 348–355.

[15] Lu, S., Liu, W., Wang, Y., Zhang, Y., Li, P., Jiang, D., Fang, C., and Li, Y., 2019, An adsorbent based on humic acid and carboxymethyl cellulose for efficient dye removal from aqueous solution, *Int. J. Biol. Macromol.*, 135, 790–797.

[16] Tiwari, D., Bhunia, H., and Bajpai, P.K., 2016, Urea-formaldehyde derived porous carbons for adsorption of CO_2, *RSC Adv.*, 6 (113), 111842–111855.

[17] Chen, S., Lu, X., Pan, F., Wang, T., and Zhang, Z., 2017, Preparation and characterization of urea-formaldehyde resin/reactive montmorillonite composites, *J. Wuhan Univ. Technol., Mater. Sci. Ed.*, 32 (4), 783–790.

[18] Liu, M., Wang, Y., Wu, Y., and Wan, H., 2018, Hydrolysis and recycling of urea formaldehyde resin residues, *J. Hazard. Mater.*, 355, 96–103.

[19] Wibowo, E.S., and Park, B.D., 2020, Determination of crystallinity of thermosetting urea-formaldehyde resins using deconvolution method, *Macromol. Res.*, 28 (6), 615–624.

[20] Nadeem, R., Manzoor, Q., Iqbal, M., and Nisar, J., 2016, Biosorption of Pb(II) onto immobilized and native *Mangifera indica* waste biomass, *J. Ind. Eng. Chem.*, 35, 185–194.

[21] Foo, K.Y., and Hameed, B.H., 2010, Insights into the modeling of adsorption isotherm systems, *Chem. Eng. J.*, 156 (1), 2–10.

[22] Arshad, M.A., Maaroufi, A., Pinto, G., El-Barkany, S., and Elidrissi, A., 2016, Morphology, thermal stability and thermal degradation kinetics of cellulose-modified urea-formaldehyde resin, *Bull. Mater. Sci.*, 39 (6), 1609–1618.

[23] Nandiyanto, A.B.D., Oktiani, R., and Ragadhita, R., 2019, How to read and interpret FTIR spectroscope of organic material, *Indones. J. Sci. Technol.*, 4 (1), 97–118.

[24] Tiwari, D., Bhunia, H., and Bajpai, P.K., 2016, Urea-formaldehyde derived porous carbons for adsorption of CO_2, *RSC Adv.*, 6 (113), 111842–111855.

[25] Shen, Y., Lin, H., Gao, W., and Li, M., 2020, The effects of humic acid urea and polyaspartic acid urea on reducing nitrogen loss compared with urea, *J. Sci. Food Agric.*, 100 (12), 4425–4432.

[26] Wang, J., and Guo, X., 2020, Adsorption kinetic models: Physical meanings, applications, and solving methods, *J. Hazard. Mater.*, 390, 122156.

[27] Li, J., and Zhang, Y., 2021, Morphology and crystallinity of urea-formaldehyde resin adhesives with different molar ratios, *Polymers*, 13 (5), 673.

[28] Zehra, T., Lim, L.B.L., and Priyantha, N., 2015, Removal behavior of peat collected from Brunei Darussalam for Pb(II) ions from aqueous solution: Equilibrium isotherm, thermodynamics, kinetics and regeneration studies, *Environ. Earth Sci.*, 74 (3), 2541–2551.

[29] Yang, X., Yang, S., Yang, S., Hu, J., Tan, X., and Wang, X., 2011, Effect of pH, ionic strength and temperature on sorption of Pb(II) on NKF-6 zeolite studied by batch technique, *Chem. Eng. J.*, 168 (1), 86–93.

[30] Dubinin, M.M., and Radushkevich, L.V., 1947, The equation of the characteristic curve of the activated charcoal, *Proc. Acad. Sci. USSR Phys. Chem. Sect.*, 55, 331–337.

[31] Tempkin, M.I., and Pyzhev, V., 1940, Kinetics of ammonia synthesis on promoted iron catalyst, *Acta Phys. Chim. USSR*, 12 (1), 327–356.

[32] Basuki, R., Yusnaidar, Y., and Rusdiarso, B., 2018, Different style of Langmuir isotherm model of non-competitive sorption Zn(II) and Cd(II) onto horse dung humic acid (HD-HA), *AIP Conf. Proc.*, 2026, 020009.

[33] Freundlich, H., 1907, Über die Adsorption in Lösungen, *Z. Phys. Chem.*, 57U (1), 385–470.

[34] Bartczak, P., Norman, M., Klapiszewski, Ł., Karwańska, N., Kawalec, M., Baczyńska, M., Wysokowski, M., Zdarta, J., Ciesielczyk, F., and

Jesionowski, T., 2018, Removal of nickel(II) and lead(II) ions from aqueous solution using peat as a low-cost adsorbent: A kinetic and equilibrium study, *Arabian J. Chem.*, 11 (8), 1209–1222.

[35] Qu, P., Li, Y., Huang, H., Wu, G., Chen, J., He, F., Wang, H., and Gao, B., 2020, Foamed urea-formaldehyde microspheres for removal of heavy metals from aqueous solutions, *Chemosphere*, 241, 125004.

[36] Kushwaha, A., Rani, R., and Patra, J.K., 2020, Adsorption kinetics and molecular interactions of lead [Pb(II)] with natural clay and humic acid, *Int. J. Environ. Sci. Technol.*, 17 (3), 1325–1336.

[37] El-Korashy, S.A., Elwakeel, K.Z., and El-Hafeiz, A.A., 2016, Fabrication of bentonite/thiourea-formaldehyde composite material for Pb(II), Mn(VII) and Cr(VI) sorption: A combined basic study and industrial application, *J. Cleaner Prod.*, 137, 40–50.

[38] Ming, G., Duan, H., Meng, X., Sun, G., Sun, W., Liu, Y., and Lucia, L., 2016, A novel fabrication of monodisperse melamine-formaldehyde resin microspheres to adsorb lead(II), *Chem. Eng. J.*, 288, 745–757.

[39] Saha, P., Chowdhury, S., Gupta, S., and Kumar, I., 2010, Insight into adsorption equilibrium, kinetics and thermodynamics of Malachite Green onto clayey soil of Indian origin, *Chem. Eng. J.*, 165 (3), 874–882.

[40] Duran, C., Ozdes, D., Gundogdu, A., and Senturk, H.B., 2011, Kinetics and isotherm analysis of basic dyes adsorption onto almond shell (*Prunus dulcis*) as a low cost adsorbent, *J. Chem. Eng. Data*, 56 (5), 2136–2147.

[41] Lagergren, S., 1898, About the theory of so called adsorption of soluble substances, *K. Sven. Vetenskapsakad. Handl.*, 24 (4), 1–39.

[42] Ho, Y.S., McKay, G., Wase, D.A.J., and Forster, C.F., 2000, Study of the sorption of divalent metal ions on to peat, *Adsorpt. Sci. Technol.*, 18 (7), 639–650.

[43] Santosa, S.J., 2014, Sorption kinetics of Cd(II) species on humic acid-based sorbent, *CLEAN - Soil Air Water*, 42 (6), 760–766.

[44] Rusdiarso, B., Basuki, R., and Santosa, S.J., 2016, Evaluation of Lagergren kinetics equation by using novel kinetics expression of sorption of Zn^{2+} onto horse dung humic acid (HD-HA), *Indones. J. Chem.*, 16 (3), 338–346.

[45] Basuki, R., Ngatijo, Santosa, S.J., and Rusdiarso, B., 2018, Comparison the new kinetics equation of noncompetitive sorption Cd(II) and Zn(II) onto green sorbent horse dung humic acid (HD-HA), *Bull. Chem. React. Eng. Catal.*, 13 (3), 475–488.

[46] Ngatijo, N., Basuki, R., Rusdiarso, B., and Nuryono, N., 2020, Sorption-desorption profile of Au(III) onto silica modified quaternary amines (SMQA) in gold mining effluent, *J. Environ. Chem. Eng.*, 8 (3), 103747.

[47] Baker, H.M., Khalili, F.I., and Aldulaimy, B.I.A., 2020, Removal of lead ions from aqueous solutions by insolubilized Iraqi humic acid, *Desalin. Water Treat.*, 206, 286–296.